Nanoflakes-Assembled Three-Dimensional Hollow-Porous V_2O_5 as Lithium Storage Cathodes with High-Rate Capacity

Liqiang Mai, Qinyou An, Qiulong Wei, Jiayang Fei, Pengfei Zhang, Xu Xu, Yunlong Zhao, Mengyu Yan, Wen Wen, and Lin Xu*

Increasing the energy density of lithium batteries requires the development of electrode materials with higher capacity,[1–5] whereby improving the cycle life involves stabilizing two critical components, namely, the active electrode materials and their interface with the electrolyte.[6] Among the potential cathode materials, vanadium pentoxide (V_2O_5) with a layered structure has been extensively investigated because of its low cost, high abundance, as well as its high energy efficiency, and relatively high theoretical capacity (about 294 mAh g^{-1} with 2 Li insertions/extractions per unit formula).[7–11] However, because of its poor structural stability and slow electrochemical kinetics, two major problems for this electrode material are the limited long-term cycling stability and low rate.[12–14]

Most strategies exploit the structure-dependent properties of nanostructured V_2O_5 for improving its electrochemical performance.[15–17] Many low-dimensional V_2O_5 nanostructures (nanoparticles,[18] nanorods,[19] nanowires,[20–23] nanotubes,[24] nanobelts,[25] nanosheets[26]) have been synthesized by various methods, and the benefits of these nanostructures have been demonstrated in mitigating the slow electrochemical kinetics and shortening the diffusion distance for Li ions. However, the low degree of freedom for volume change during the Li ions intercalation and de-intercalation processes is still a critical problem for low-dimensional nanostructures. Three-dimensional (3D) hollow structures have attracted considerable attention as an important family of electrode materials in recent years.[27–31] Especially, hollow-porous nanostructures, with a hollow interior and porous shell, not only possess the advantages of low-dimensional nanomaterials, but also provide a more effective free volume for the uniform distribution of the induced stress and strain (**Figure 1**a).[32–35] In this work, we present a morphology-controlled synthesis of nanoflakes-assembled 3D hollow-porous V_2O_5 (HP-V_2O_5) quasi-microspheres via a facile solvothermal and annealing method. This approach can be extended to the synthesis of other transition metal oxide electrode materials. When evaluated as a cathode material for Li-ion storage, the as-synthesized HP-V_2O_5 manifests a high-rate capacity and good cycling performance.

The fabrication of HP-V_2O_5 quasi-microspheres is relatively facile and involves the following steps (Figure 1b,c). Firstly, carbon microspheres (CMs) with diameters of 2–4 μm (Figure S1, Supporting Information) were prepared by a hydrothermal method. The second step was the preparation of CM@VO composite quasi-microspheres (Figure S2 and S3, Supporting Information) using CMs as the template, ammonium metavanadate (NH_4VO_3) as the vanadium source, and urea as the pore-forming surfactant. During the solvothermal reaction numerous precursor nucleus formed quickly on the surface of the CMs and then grew into flake-like nanocrystals. Extending the reaction time resulted in a further aggregation of the precursors, which developed into microsized core–shell composites composed of a CM core and a vanadium oxide nanosheets shell. Finally, the HP-V_2O_5 quasi-microspheres were prepared by calcination of the CM@VO composites at 450 °C for 2 h. In this process, the removal of the CM template and the oxidation of VO (Figure S4, Supporting Information) resulted in the formation of the V_2O_5 hollow structure. During this process the nanosheets were split into innumerable nanoflakes owing to the release of NH_3 and CO_2, which resulted from the decomposition of residual urea (Figure S5, Supporting Information) and the CMs, respectively, under the thermal treatment. Therefore, the obtained hollow V_2O_5 quasi-microspheres are highly porous.

The morphology and microstructure of the HP-V_2O_5 quasi-microspheres were characterized by field-emission scanning electron microscopy (FESEM) and transmission electron microscopy (TEM) respectively. The FESEM images (**Figure 2**a,b) reveal that the product is composed of hedgehog-like V_2O_5 quasi-microspheres with a diameter in the range of

Prof. L. Q. Mai, Q. Y. An, Q. L. Wei, P. F. Zhang, X. Xu, Y. L. Zhao, M. Y. Yan, W. Wen, Dr. L. Xu
WUT-Harvard Joint Nano Key Laboratory
State Key Laboratory of Advanced Technology for Materials Synthesis and Processing
Wuhan University of Technology
Wuhan 430070, P. R. China
E-mail: mlq518@whut.edu.cn
Dr. L. Xu
Department of Chemistry and Chemical Biology
Harvard University
Cambridge, Massachusetts 02138, USA
J. Y. Fei
Department of Materials Science and Engineering
University of Pennsylvania
Philadelphia, Pennsylvania 19104, USA

DOI: 10.1002/smll.201302991

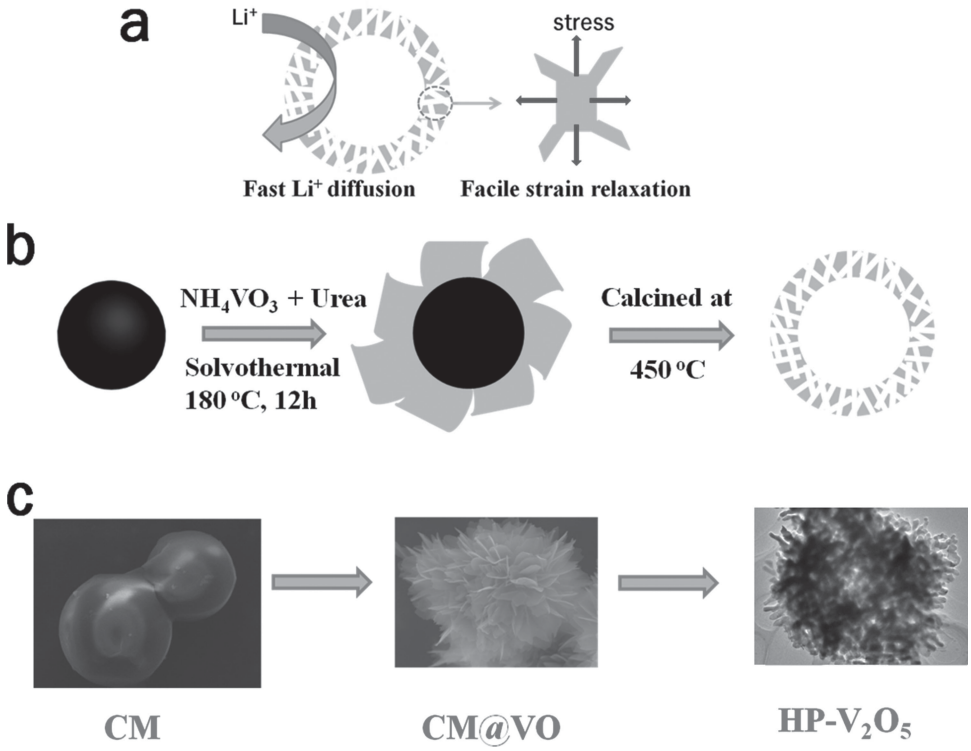

Figure 1. a) The hollow-porous structure provides an effective electrode–electrolyte contact area, which shortens the ion-diffusion pathway, and a facile strain relaxation for swelling during lithiation/delithiation. b) Schematic illustration and c) corresponding morphologies in the fabrication process of nanoflakes-assembled HP-V_2O_5.

3–6 μm. It is interesting to observe that a significant fraction of the hedgehog-like V_2O_5 quasi-microspheres have cracks on their surface. A typical broken hollow quasi-microsphere is shown in Figure 2c, and the hollow interior can be clearly observed from the broken part. The broken quasi-microsphere reveals that the wall of the hedgehog-like V_2O_5 hollow quasi-microspheres is porous and composed of nano-sized subunits (nanoflakes). The wall thickness of the hollow-porous quasi-microspheres is determined to be about 500 nm. Representative TEM images (Figure 2d) of the HP-V_2O_5 further confirm the hollow-porous structure with nanoflakes pointing out from the surface.

The presence of nanoflakes can clearly be seen in Figure 2e. From a high-resolution TEM (HRTEM) image taken from the edge of a nanoflake (Figure 2f), the lattice fringes are clearly visible with spacings of 3.40 and 4.08 Å, which are in agreement with those of the (110) and (101) planes of V_2O_5 (JCPDS card No. 03–065–0131). The corresponding fast-Fourier transform (FFT) pattern (Figure 2g) of the lattice-fringe pattern demonstrates well-resolved individual reflections, which indicates that the flakes are single crystalline. As determined by N_2-sorption measurements (Figure S4, Supporting Information), these hollow-porous

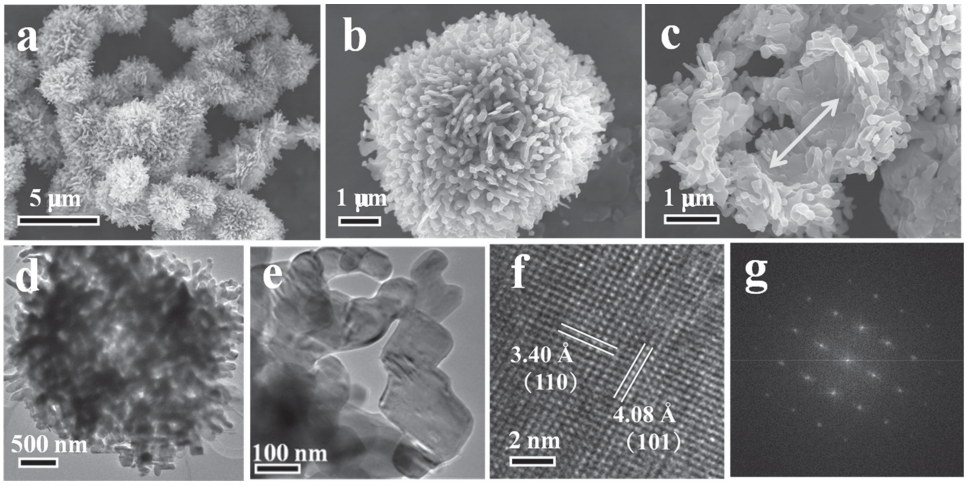

Figure 2. a–c) FESEM images, d,e) TEM images, f) HRTEM image, and g) FFT pattern of nanoflakes-assembled HP-V_2O_5 quasi-microspheres.

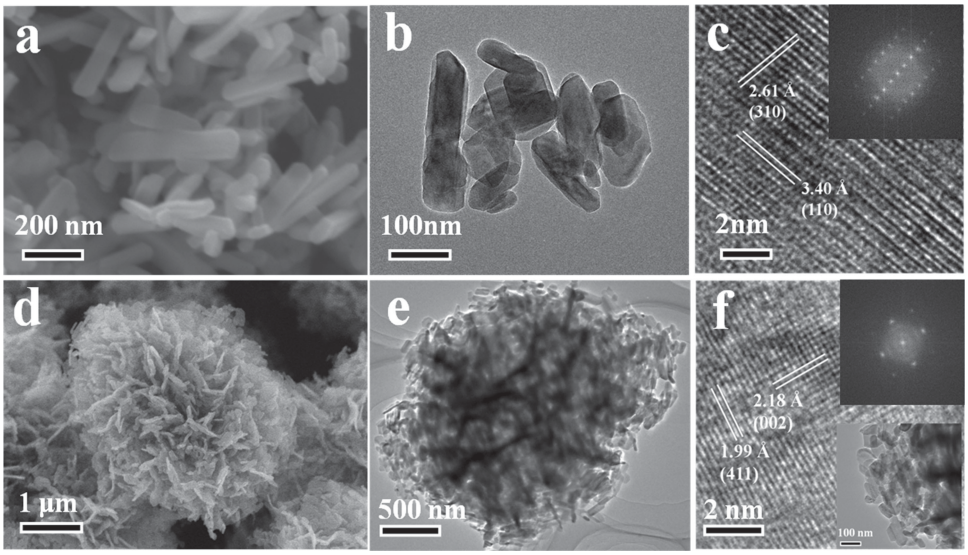

Figure 3. a) FESEM, b) TEM, and c) HRTEM images of R-V_2O_5; the inset of Figure 3c is the FFT pattern on a selected area. d) FESEM, e) TEM, and f) HRTEM images of P-V_2O_5; the insets of Figure 3f are the high-magnification TEM image (lower part) and the FFT pattern (upper part).

structures hold a Brunauer-Emmett-Teller (BET) surface area of 8.6 m^2 g^{-1} and a relatively high pore volume of 0.15 cm^3 g^{-1}, the latter mainly being contributed from the macropores between the V_2O_5 nanoflakes. The reaction time, concentration of the reactants, and type of solvent of the solvothermal reaction process play, as expected, an important role on the morphology and structure of the products (Figure S7–S9, Supporting Information). In addition, based on the thermal decomposition reaction, the calcination temperature also plays a significant role in the formation process of HP-V_2O_5 (Figure S10, Supporting Information).

To further investigate the growth details of the samples, we carried out the synthesis of V_2O_5 under different conditions. First, V_2O_5 nanorods (R-V_2O_5, **Figure 3**a) were synthesized by adding NH_4VO_3 in an ethylene glycol (EG)/water solution and keeping the other synthesis parameters similar to the ones above that resulted in the growth of HP-V_2O_5. Sample R-V_2O_5 mainly consists of nanorods with diameters from 80 to 100 nm (Figure 3b). The HRTEM image and FFT pattern (Figure 3c) confirm that the nanorods have well-resolved lattice planes. In order to understand the important role of CM during the growth of the HP-V_2O_5, the V_2O_5 porous structure (P-V_2O_5, Figure 3d) was synthesized in the absence of CM and again the other synthesis parameters were kept similar to the ones above that resulted in the growth of HP-V_2O_5. The TEM image (Figure 3e) of the P-V_2O_5 sample reveals the porous nature of the quasi-microsphere, which is composed of small nanoflakes (lower inset of Figure 3f). Well-resolved lattice planes can be identified in the HRTEM image (Figure 3f) of P-V_2O_5. Hollow V_2O_5 spheres could also be obtained by adding CMs as hard templates (without urea). The SEM image (Figure S11, Supporting Information) demonstrates collapsed V_2O_5 spheres with a hollow structure.

The resultant products (HP-V_2O_5, P-V_2O_5, and R-V_2O_5) were all characterized by X-ray diffraction (XRD) to identify the crystallographic structure and crystallinity (Figure S12, Supporting Information). All three patterns could be assigned to well-crystallized orthorhombic V_2O_5 (JCPDS Card No. 03–065–0131, space group: *Pmmn*) and no other diffraction peaks exists, implying that the products are pure V_2O_5. The sharp and intense diffraction peaks indicate a high crystallization degree of the products.

The electrochemical behavior of the as-prepared V_2O_5 electrodes was evaluated using a CR2025-type coin cell. The cyclic voltammetry (CV) measurements for samples R-V_2O_5, P-V_2O_5, and HP-V_2O_5 were carried out at a scan rate of 0.1 mV s^{-1} in the potential range from 4.0 to 2.0 V vs Li/Li^+ at room temperature (**Figure 4**a). The cathodic and anodic peaks can be ascribed to the Li ions insertion and extraction processes at the cathodes, respectively. The shapes of the three curves are almost identical, and three main cathodic peaks appear at potentials of 3.3, 3.1, and 2.2 V (vs Li/Li^+) in the CV curves. HP-V_2O_5 has a larger area under the curve and a higher redox peak current than those of samples R-V_2O_5 and P-V_2O_5, suggesting that HP-V_2O_5 has the highest capacity and the fastest kinetics for Li ions insertion/extraction.[36] The cathodic performance of the as-prepared V_2O_5 nanomaterials was evaluated by galvanostatic discharge/charge testing. Figure 4b displays the initial discharge/charge curves of the V_2O_5 nanomaterial cathodes at the current density of 100 mA g^{-1}. Three voltage plateaus related to different redox reactions that can be associated with Li ions insertion are clearly observed in the discharge curves. The first two plateaus at approximately 3.3 and 3.1 V can be ascribed to the phase transitions from α-V_2O_5 to ε-$Li_{0.5}V_2O_5$ and δ-LiV_2O_5, corresponding to Equation (1) and (2),[37] respectively. The combined discharge capacity related to these phase transitions is over 140 mAh g^{-1}, which is consistent with the theoretical value of 147 mAh g^{-1} for the formation of δ-LiV_2O_5. The plateau at approximately 2.2 V can be attributed to the generation of γ-$Li_2V_2O_5$, resulting from further lithium insertion into LiV_2O_5 (Equation (3)).

$$V_2O_5 + 1/2Li^+ + 1/2e^- = \varepsilon - Li_{0.5}V_2O_5 \quad (1)$$

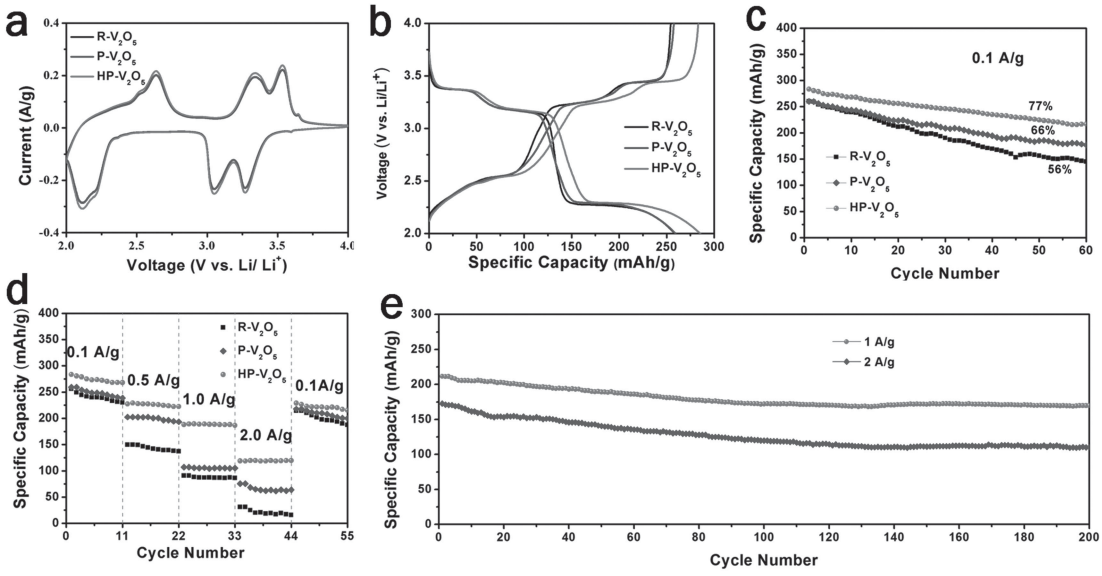

Figure 4. Electrochemical properties of as-prepared R-V_2O_5, P-V_2O_5, and HP-V_2O_5 electrodes. a) Cyclic voltammetry curves at a scan rate of 0.1 mV s^{-1} in the potential range from 4.0 to 2.0 V vs. Li/Li^+. b,c) The initial charge–discharge curves (b) and the cycling performance (c) at the current density of 100 mA g^{-1}. d) Rate property of different samples at various current densities from 100 to 2000 mA g^{-1}. e) The cycling performance of a HP-V_2O_5 electrode at high rates.

$$\varepsilon - Li_{0.5}V_2O_5 + 1/2Li^+ + 1/2e^- = \delta - LiV_2O_5 \quad (2)$$

$$\delta - LiV_2O_5 + Li^+ + e^- = \gamma - Li_2V_2O_5 \quad (3)$$

Figure 4c is the cycling performance comparison of the three samples at the current density of 100 mA g^{-1}. The initial discharge capacity of samples R-V_2O_5, P-V_2O_5, and HP-V_2O_5 were 260, 260, and 283 mAh g^{-1} (theoretical capacity: 294 mAh g^{-1}), respectively. The discharge capacities decreased to 145, 177, and 217 mAh g^{-1} after 60 cycles, corresponding to capacity retentions of 56%, 66%, and 77%, respectively. It is obvious that sample HP-V_2O_5 exhibits the highest capacity and best cycling performance. To better understand the advantage of the hollow-porous structures for lithium storage, the rate performances of the three samples were also compared (Figure 4d). It can clearly be seen that, compared to the R-V_2O_5 and P-V_2O_5 samples, the specific capacity of the HP-V_2O_5 sample is substantially higher at all investigated discharge rates from 100 to 2000 mA g^{-1}. For example, the HP-V_2O_5 electrode exhibits a much superior rate performance of 189 and 119 mAh g^{-1}, which is over two times larger than that of the R-V_2O_5 electrode (87 and 31 mAh g^{-1}) at current densities of 1000 and 2000 mA g^{-1}, respectively. This result is also better than those of previously reported V_2O_5 quantum dots/graphene hybrid nanocomposites,[38] spherical porous V_2O_5,[39] and V_2O_5/poly(3,4-ethylenedioxythiophene) and MnO_2 nanowires.[21] Importantly, the high capacity of the hollow-porous electrode can be retained at 227 mAh g^{-1} (80% of the initial values) at 100 mA g^{-1} even after 55 high-rate cycles. This performance confirms the excellent structural stability and the resulting high reversibility of the V_2O_5 hollow-porous structure.

The high-rate capability of the hollow-porous V_2O_5 cathode was further investigated (Figure 4e). The initial specific discharge capacities were 212 and 173 mAh g^{-1} at current densities of 1 and 2 A g^{-1}, respectively. After 200 cycles, the capacity at 1 A g^{-1} decreased to 170 mAh g^{-1}, corresponding to a capacity fading of 0.11% per cycle; the capacity at 2 A g^{-1} decreased to 111 mAh g^{-1}, corresponding to a capacity fading of 0.22% per cycle. At the same time, the coulombic efficiencies both remained at around 100% in the overall battery operation, indicating a good reversibility (Figure S13, Supporting Information). The electrochemical performance of the HP-V_2O_5 microstructures is much better than those of previously reported V_2O_5 nanoparticles,[40] porous structures,[41] and nanotubes.[42] It is even better than that of a V_2O_5 nanowire/CNT composite electrode reported recently.[43] The HP-V_2O_5 quasi-microsphere exhibits an excellent rate capability as compared to the R-V_2O_5 and P-V_2O_5 samples, however, the difference in conductivity between them should be taken into account.[33] Electrochemical impedance spectroscopy (EIS) measurements were performed to study and compare the conductivity[33] of the cathodes composed of HP-V_2O_5, P-V_2O_5, and R-V_2O_5 (Figure S14, Supporting Information). It is clear from these results that the HP-V_2O_5 electrode possesses a much lower resistance than that of the R-V_2O_5 and P-V_2O_5 electrodes (ca. 150 Ω vs. 170 and 250 Ω, respectively), thus indicating that the incorporation of a hollow-porous structure can significantly enhance the electrochemical kinetics.

The improved rate capability and cycling stability are attributed to the interesting 3D hollow-porous structure. More specifically, the porous shell of the structure seems to facilitate the electrolyte penetration and increase the contact area between the HP-V_2O_5 electrode material and the electrolyte.[44] The V_2O_5 nanoflakes with many spaces between them have an increased portion of exposed surfaces, which ensure a higher utilization of electrode materials and provide more electrochemically active sites for Li ions

to access, thus a high capacity is achieved.[45] Moreover, the hollow-porous structure might also be an advantage to accommodate the volume variation during the Li ions intercalation and deintercalation.[33] Finally, the nanosized building blocks reduce the distance for Li ions diffusion and electron transport.[44,46] In brief, the synergistic effect of the successful integration of the V_2O_5 hollow structure with a porous structure is beneficial to the improved cycling stability and excellent rate capability of our HP-V_2O_5 quasi-microspheres.

In summary, nanoflakes-assembled 3D hollow-porous V_2O_5 quasi-microspheres have been successfully synthesized by a facile solvothermal method followed by annealing at 450 °C in air. The morphology of the V_2O_5 can be tailored by adjusting the solvothermal reaction conditions and calcination temperature. The resulting HP-V_2O_5 microspheres deliver promising Li-storage property with high specific capacity, stable cyclability, and good rate performance. Employed as the cathode they attain a specific capacity of 173 mAh g^{-1} at 2 A g^{-1}, which is attractive for the development of Li batteries with high power densities and high energy densities. The excellent electrochemical performance are attributed to the nanosized building blocks of the 3D V_2O_5 hollow-porous structure, which provides a short Li ions diffusion distance, effective strain relaxation, and large active contact area. Furthermore, the synthesis strategy demonstrated herein is facile and versatile for the fabrication and application of other transition metal oxide electrode materials.

Experimental Section

Materials Synthesis: The carbon microspheres were synthesized by a hydrothermal method.[47] In a typical experiment, the as-prepared carbon spheres were utilized as hard templates, NH_4VO_3 was used as precursor, and urea as the structure-directing agent. The specific steps are described below. First, 110 mg of carbon spheres were added into ethylene glycol (EG) (40 mL) and stirred vigorously for 5 min, then ultrasonicated at 40 Hz for 20 min. Sequentially, urea (1.5 g) was dissolved in 10 mL deionized water and stirred for 5 min, then NH_4VO_3 (110 mg) was added into the solution and heated to 80 °C in a water bath to obtain a homogeneous solution. The solution was the mixed with the suspension containing the carbon spheres and the new suspension was kept under stirring for another 2.5 h at 80 °C in a water bath. When all the raw materials were spread homogeneously, the mixture was sealed into a 100 mL Teflon-lined stainless steel autoclave and then solvothermally treated for 12 h at 180 °C. Following precipitate isolation and drying, the samples were annealed at 450 °C for 2 h in air.

Characterization: XRD measurements were performed to investigate the crystallographic information using a D8 Advance X-ray diffractometer with a non-monochromated Cu Kα X-ray source. FESEM images were collected with a Hitachi S-4800 microscope at an acceleration voltage of 10 kV. TEM and HRTEM images were recorded using a JEM-2100F STEM/EDS microscope. BET surface areas were measured using a Gemini 2360 instrument to determine the adsorption of nitrogen.

Measurement of Electrochemical Performance: The electrochemical measurements were carried out using 2025 coin cells in a glove box filled with pure argon gas, using a lithium pellet as the anode, a 1 m solution of $LiPF_6$ in ethylene carbon (EC)/dimethyl carbonate (DMC) as the electrolyte, and the cathode electrodes were obtained using 70% hollow-porous V_2O_5 active material, 20% acetylene black, and 10% poly(tetrafluoroethylene) (PTFE). Galvanostatic charge/discharge cycling was studied in a potential range of 4.0–2.0 V vs. Li/Li^+ with a multichannel battery testing system (LAND CT2001A). Cyclic voltammetry (CV) and AC-impedance spectra were recorded using an electrochemical workstation (Autolab PGSTAT 302 and CHI 760D).

Supporting Information

Supporting Information is available from the Wiley Online Library or from the author.

Acknowledgements

This work was supported by the National Basic Research Program of China (2013CB934103, 2012CB933003), the National Natural Science Foundation of China (51072153, 51272197) and the Program for New Century Excellent Talents in University (NCET-10–0661). Thanks to Prof. C.M. Lieber of Harvard University, Prof. Dongyuan Zhao of Fundan University, and Dr. Jun Liu of Pacific Northwest National Laboratory for their strong support and stimulating discussions.

[1] M. Armand, J. M. Tarascon, *Nature* **2008**, *451*, 652.
[2] J. B. Goodenough, Y. Kim, *Chem. Mater.* **2009**, *22*, 587.
[3] B. Kang, G. Ceder, *Nature* **2009**, *458*, 190.
[4] M. S. Whittingham, *Chem. Rev.* **2004**, *104*, 4271.
[5] J. M. Tarascon, M. Armand, *Nature* **2001**, *414*, 359.
[6] H. Wu, G. Chan, J. W. Choi, I. Ryu,Y. Yao, M. T. McDowell, S. W. Lee, A. Jackson, Y. Yang, L. B. Hu, Y. Cui, *Nat. Nanotechnol.* **2012**, *7*, 310.
[7] S. Q. Wang, S. R. Li, Y. Sun, X. Y. Feng, C. H. Chen, *Energy Environ. Sci.* **2011**, *4*, 2854.
[8] Q. T. Qu, Y. S. Zhu, X. W. Gao, Y. P. Wu, *Adv. Energy Mater.* **2012**, *2*, 950.
[9] S. Zhou, X. G. Yang, Y. J. Lin, J. Xie, D. W. Wang, *ACS Nano* **2012**, *6*, 919.
[10] Y. Wang, G. Z. Cao, *Adv. Mater.* **2008**, *20*, 2251.
[11] T. Y. Zhai, H. M. Liu, H. Q. Li, X. S. Fang, M. Y. Liao, L. Li, H. S. Zhou, Y. Koide, Y. Bando, D. Golberg, *Adv. Mater.* **2010**, *22*, 2547.
[12] C. Ban, N. A. Chernova, M. S. Whittingham, *Electrochem. Commun.* **2009**, *11*, 522.
[13] J. Muster, G. T. Kim, V. Krstic, J. G. Park, Y. W. Park, S. Roth, M. Burghard, *Adv. Mater.* **2000**, *12*, 420.
[14] T. Watanabe, Y. Ikeda, T. Ono, M. Hibino, M. Hosoda, K. Sakai, T. Kudo, *Solid State Ionics* **2002**, *151*, 313.
[15] X. Y. Chen, E. Pomerantseva, P. Banerjee, K. Gregorczyk, R. Ghodssi, G. Rubloff, *Chem. Mater.* **2012**, *24*, 1255.
[16] A. Q. Pan, H. B. Wu, L. Yu, T. Zhu, X. W. Lou, *ACS Appl. Mater. Interfaces* **2012**, *4*, 3874.

[17] Y. L. Cheah, V. Aravindan, S. Madhavi, *ACS Appl. Mater. Interfaces* **2013**, *5*, 3475.
[18] S. H. Ng, T. J. Patey, R. Buechel, F. Krumeich, J. Z. Wang, H. K. Liu, S. E. Pratsinis, *Phys. Chem. Chem. Phys.* **2009**, *11*, 3748.
[19] K. Takahashi, S. J. Lim, Y. Wang, G. Z. Cao, *Jpn. J. Appl. Phys., Part 1* **2005**, *44*, 662.
[20] L. Q. Mai, L. Xu, C. H. Han, X. Xu, Y. Z. Luo, S. Y. Zhao, Y. L. Zhao, *Nano Lett.* **2010**, *10*, 4750.
[21] L. Q. Mai, F. Dong, X. Xu, Y. Z. Luo, Q. Y. An, Y. L. Zhao, J. Pan, J. N. Yang, *Nano Lett.* **2013**, *13*, 740.
[22] L. Q. Mai, X. Xu, L. Xu, C. H. Han, Y. Z. Luo, *J. Mater. Res.* **2011**, *26*, 2175.
[23] H. M. Liu, W. S. Yang, *Energy Environ. Sci.* **2011**, *4*, 4000.
[24] Y. Wang, K. Takahashi, H. M. Shang, G. Z. Cao, *J. Phys. Chem. B* **2005**, *109*, 3085.
[25] H. Wang, K. Huang, C. Huang, S. Liu, Y. Ren, X. Huang, *J. Power Sources* **2011**, *196*, 5645.
[26] X. H. Rui, Z. Y. Lu, H. Yu, D. Yang, H. H. Hng, T. M. Lim, Q. Y. Yan, *Nanoscale* **2013**, *5*, 556.
[27] Z. Y. Wang, L. Zhou, X. W. Lou, *Adv. Mater.* **2012**, *24*, 1903.
[28] J. S. Chen, X. W. Lou, *Small* **2011**, *1*, 1877.
[29] Y. M. Wu, Z. H. Wen, H. H. Feng, J. H. Li, *Small* **2012**, *8*, 858.
[30] G. L. Cui, Y. S. Hu, L. J. Zhi, D. Q. Wu, I. Lieberwirth, J. Maier, K. Müllen, *Small* **2007**, *3*, 2066.
[31] D. Mao, J. X. Yao, X. Y. Lai, M. Yang, J. Du, D. Wang, *Small* **2011**, *7*, 578.
[32] Y. Yao, M. T. McDowell, I. Ryu, H. Wu, N. Liu, L. Hu, W. D. Nix, Y. Cui, *Nano Lett.* **2011**, *11*, 2949.
[33] D. Y. Chen, X. Mei, G. Ji, M. H. Lu, J. P. Xie, J. M Lu, J. Y. Lee, *Angew. Chem. Int. Ed.* **2012**, *51*, 2409.
[34] A. Vu, Y. Q. Qian, A. Stein, *Adv. Energy Mater.* **2012**, *3*, 1056.
[35] J. Zheng, B. H. Wu, Z. Y. Jiang, Q. Kuang, X. L. Fang, Z. X. Xie, R. B. Huang, L. S. Zheng, *Chem. Asian J.* **2010**, *5*, 1439.
[36] X. Xu, Y. Z. Luo, L. Q. Mai, Y. L. Zhao, Q. Y. An, L. Xu, F. Hu, L. Zhang, Q. J. Zhang, *NPG Asia Mater.* **2012**, *4*, e20.
[37] X. F. Zhang, K. X. Wang, X. Wei, J. S. Chen, *Chem. Mater.* **2011**, *23*, 5290.
[38] C. H. Han, M. Y. Yan, L. Q. Mai, X. C. Tian, L. Xu, X. Xu, Q. Y. An, Y. L. Zhao, X. Y. Ma, J. L. Xie, *Nano Energy* **2013**, doi: 10.1016/j.nanoen.2013.03.012.
[39] C. Q. Feng, S. Y. Wang, R. Zeng, Z. P. Guo, K. Konstantinov, H. K. Liu, *J. Power Sources* **2008**, *184*, 485.
[40] S. Ng, T. J. Patey, R. Buchel, F. Krumeich, J. Wang, H. K. Liu, S. E. Pratsinis, P. Novak, *Phys. Chem. Chem. Phys.* **2009**, *11*, 3748.
[41] J. J. Yu, J. Yang, W. B. Nie, Z. H. Li, E. H. Liu, G. T. Lei, Q. Z. Xiao, *Electrochim. Acta* **2013**, *89*, 292.
[42] Y. Wang, K. Takahashi, H. M. Shang, G. Z. Cao, *J. Phys. Chem. B* **2005**, *109*, 3085.
[43] X. L. Jia, Z. Chen, A. Suwarnasarn, L. Rice, X. L. Wang, H. Sohn, Q. Zhang, B. M. Wu, F. Wei, Y. F. Lu, *Energy Environ. Sci.* **2012**, *5*, 6845.
[44] N. Jayaprakash, J. Shen, S. S. Moganty, A. Corona, L. A. Archer, *Angew. Chem. Int. Ed.* **2011**, *50*, 5904.
[45] A. Q. Pan, T. Zhu, H. B. Wu, X. W. Lou, *Chem. Eur J.* **2013**, *19*, 494.
[46] S. Q. Wang, Z. D. Lu, D. Wang, C. G. Li, C. H. Chen, Y. D. Yin, *J. Mater. Chem.* **2011**, *21*, 6365.
[47] X. M. Sun, Y. D. Li, *Angew. Chem. Int. Ed.* **2004**, *43*, 597.

Received: September 15, 2013
Published online: April 7, 2014

